Liquid-liquid phase transition in a two-dimensional system with anomalous liquid properties

Tomaz Urbic
Faculty of Chemistry and Chemical Technology, University of Ljubljana, 1000, Slovenia
(Received 25 June 2013; revised manuscript received 3 October 2013; published 6 December 2013)

The phase diagram of the two-dimensional particles interacting through a smooth version of Stell-Hemmer interaction was studied using Monte Carlo computer simulations. By evaluating the pressure-volume isotherms, we observed liquid-liquid, liquid-gas phase transitions and three stable crystal phases. The model shows the liquid-liquid critical point in stable liquid phase and is confirmed by observing properties of other thermodynamic functions such as heat capacity and isothermal compressibility, for example. The liquid-gas and the liquid-liquid critical points were estimated within the thermodynamic limit.

DOI: 10.1103/PhysRevE.88.062303 PACS number(s): 64.70.Ja, 61.20.Ja

I. INTRODUCTION

Core-softened potentials were first proposed by Stell and Hemmer in 1970 [1]. In their work, they proposed the possibility of a second critical point in addition to a standard liquid-gas critical point, if interaction potentials have a region of negative curvature. Order parameter is important in physics of phase transitions. In the case of phase transition between two phases, this order parameter can be the difference in densities of both phases in equilibrium. In simple liquids, like particles interacting by Lennard-Jones potential there is only one critical point possible. The phase transition is a consequence of two parts of potential, attraction, and repulsion. If the intermolecular potential of the fluid exhibits two characteristic distances such as two minima, then we can have another critical point as a consequence of interplay between these two distances. As it has been shown before, core-softened potentials, and similar shouldered potentials, are of particular importance, for they can reproduce various fluid anomalies that are typical for water and other substances with angular-dependent interactions [2–4], such as silica [3], silicon [5], and BeF_2 [6]. Core-softened potentials were used to study single-component liquid metal systems [7–11]. After a liquid-liquid phase transition was suggested as an explanation for water's anomalous properties by Poole *et al.* [12], there was increasing interest in studies of such transitions. Various studies have been done to understand the liquid-liquid phase transition and its associated properties [13–24]. Franzese *et al.* [25] showed that the reason for liquid-liquid phase transition and its critical point might be due to potential with two characteristic distances (hard code and soft core). In their work, they reported the existence of the low-density liquid phase and the high-density liquid phase obtained for a three-dimensional (3D) model using molecular dynamics (MD) simulations. On the other hand, two-dimensional (2D) MD produced only a density anomaly but no liquid-liquid phase transition [26,27]. Scala *et al.* [28] carried out MD simulations of 2D discrete and smoothed versions of potential to study liquid anomalies. These studies were continued by Buldyrev *et al.* [13] to explore the liquid-liquid phase transition for 2D and 3D versions of potentials and by Almudallal *et al.* [14]. They both produced phase diagrams for a discrete version of potential with liquid anomalies, and no liquid-liquid critical point in the stable liquid region was obtained. The main difference between their work and our work is usage of a different simulation method, in our case Monte Carlo simulation. Our Monte Carlo (MC) results are in agreement with their reported results for the supercritical part, but they do not agree for the subcritical part.

This paper is organized as follows. First, we present a core-softened model. In the next section we present Monte Carlo simulation details. In the Results section, we present MC calculations of the phase diagram and critical point. In addition, we provide different checks for validation of the liquid-liquid phase transition obtained from MC simulations.

II. MODEL

In this work we use the smooth version of the core-softened potential proposed by Scala *et al.* [28]. The interaction potential between 2D particles $U(r)$ is calculated by adding a Gaussian well to the Lennard-Jones (LJ) part of the potential,

$$U(r) = U_{LJ}(r) + U_1(r), \tag{1}$$

where $U_{LJ}(r)$ is standard Lennard-Jones potential and is defined as

$$U_{LJ}(r) = 4\varepsilon\left[\left(\frac{\sigma}{r}\right)^{12} - \left(\frac{\sigma}{r}\right)^{6}\right], \tag{2}$$

where ε is the well depth and σ the contact parameter of LJ potential. The Gaussian part of the interaction is

$$U_1(r) = -\lambda\varepsilon \exp\left[-a\left(\frac{r - r_0}{\sigma}\right)^2\right]. \tag{3}$$

For the sake of comparison with the previous studies, we adopt the units and values of model parameters as used before by Scala *et al.* [28]. We use $\varepsilon = 1.0$, $\sigma = 1.0$, $\lambda = 1.7$, $a = 25.0$, and $r_0 = 1.5\sigma$. Figure 1 shows the shape of the smooth version of the core-softened potential.

III. MONTE CARLO SIMULATION

A 2D system of particles was studied by the Monte Carlo simulation method in the isothermal-isobaric (NpT) ensemble, and in the canonical (NVT) ensemble. We calculated thermodynamic and structural properties of the model. All simulations were performed with $N = 100$, 200, 300, or 400 molecules because a finite size scale analysis is important for validity of critical points. 100 particles in 2D is the equivalent of 1000 particles in 3D and 400 is equivalent to 8000. It is well known that small systems favor phase separation which

 ©2013 American Physical Society

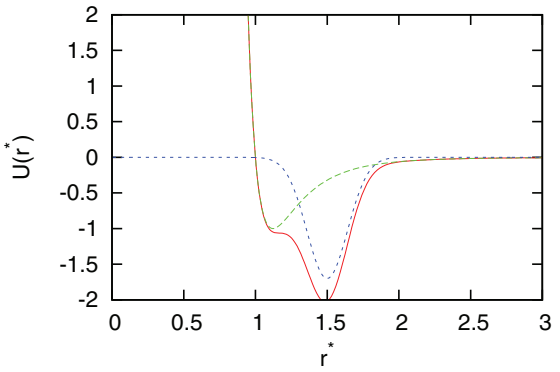

FIG. 1. (Color online) The core-softened potential $U(r)$ (solid line), LJ contribution (long dashed line), and Gaussian part (dashed line).

might not be present in the thermodynamic limit. At each step, the displacements in the x,y coordinates were chosen randomly. We used periodic boundary conditions and the minimum image convention to mimic an infinite system of particles. The starting configurations were selected at random. In the ensemble for every 10 passes, an attempt is made to scale the dimensions of the box, and all of its component particles, to hold the pressure constant. The maximum volume change and particle displacement were calibrated during equilibration simulations. 5×10^4 moves per particle were needed to equilibrate the system. The statistics were gathered over the next 1×10^6 moves to obtain well-converged results. The mechanical properties such as energy, enthalpy, and volume were calculated as the statistical averages of these quantities over the course of the simulations [29]. The heat capacity c_p and c_v, the isothermal compressibility κ, and the thermal expansion coefficient α were computed from the fluctuation formulas [30] of energy U, enthalpy H, and volume V [30]:

$$C_V = \frac{\langle U^2\rangle - \langle U\rangle^2}{NT^2}, \quad C_p = \frac{\langle H^2\rangle - \langle H\rangle^2}{NT^2},$$
$$\kappa = \frac{\langle V^2\rangle - \langle V\rangle^2}{T\langle V\rangle}, \quad \alpha = \frac{\langle VH\rangle - \langle V\rangle\langle H\rangle}{T^2\langle V\rangle}. \tag{4}$$

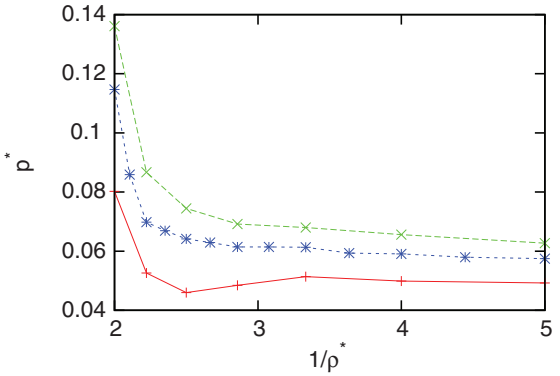

FIG. 2. (Color online) p-V isotherms for $T^* = 1.05$ (red), for $T^* = 1.08$ (blue), and $T^* = 1.10$ (green) for 200 particles in the simulation box.

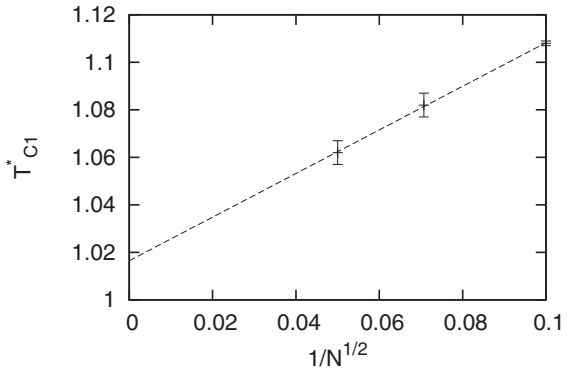

FIG. 3. Dependence of critical temperature T^*_{C1} on reverse square number of particles in simulation box.

IV. RESULTS AND DISCUSSION

We present our results below in dimensionless units, normalized to the LJ interaction parameter ε and characteristic length σ. The excess internal energy, enthalpy, and temperature are normalized as $U^* = \frac{U}{\varepsilon}$, $H^* = \frac{H}{\varepsilon}$, $T^* = \frac{k_B T}{\varepsilon}$, all the distances ($r^* = \frac{r}{\sigma}$), volume ($V^* = V/\sigma^2$), and pressure ($p^* = p\sigma^2/\epsilon$).

First we calculated both critical points, liquid-gas and liquid-liquid critical points. Figure 2 shows isotherms around the liquid-gas critical point for 200 particles in the simulation box and Fig. 3 estimation of thermodynamic limit. By extrapolation and within the thermodynamic limit we estimated that the liquid-gas critical point (C1) is at $T^*_{C1} = 1.016 \pm 0.002$, $p^*_{C1} = 0.039 \pm 0.002$, and $\rho^*_{C1} = 0.300 \pm 0.003$. A finite system behaves differently than the corresponding infinite system. Energy per particle decreases with increasing particle size or size of the simulation box. This means that the location of the critical point is different for different system sizes. There are also other size effects that can affect the critical behavior. When the system approaches the critical point, there are fluctuations of all sizes in the system and a disturbance in one point of the system can easily propagate and affect the entire system. The correlation length increases and for an infinite system goes to infinity as the critical temperature is approached. For finite-sized systems the correlation length reaches the system size before the critical point of an infinite system is reached.

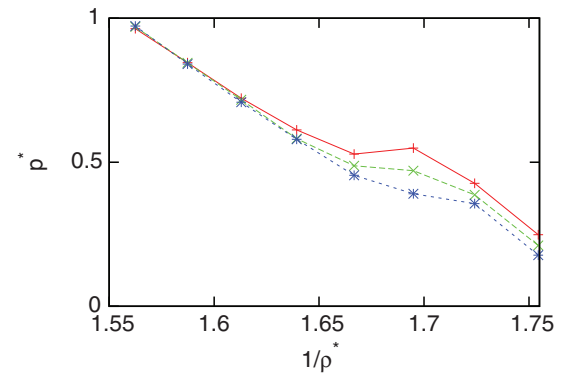

FIG. 4. (Color online) p-V isotherms for $T^* = 0.62$ (red), $T^* = 0.63$ (green), and for $T^* = 0.64$ (blue) for 200 particles in the simulation box.

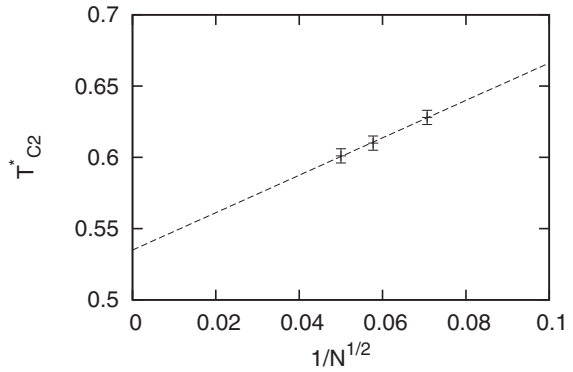

FIG. 5. Dependence of critical temperature T^*_{C1} on reverse square number of particles in simulation box.

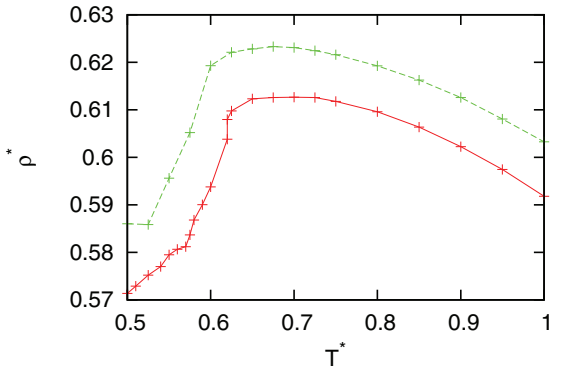

FIG. 8. (Color online) Temperature dependence of density at constant pressure for $p^* = 0.6$ (red) and $p^* = 0.75$ (green).

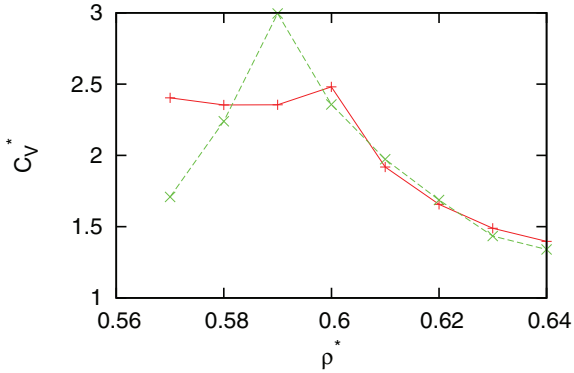

FIG. 6. (Color online) Heat capacity at constant volume for $T^* = 0.610$ (red), which is below critical point, and for $T^* = 0.611$ (green), which is a temperature above the critical point, for a 300-particle system in a simulation box.

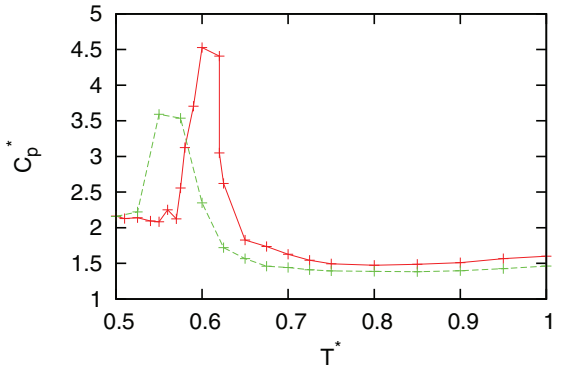

FIG. 9. (Color online) Temperature dependence of heat capacity at constant pressure for $p^* = 0.6$ (red) and $p^* = 0.75$ (green).

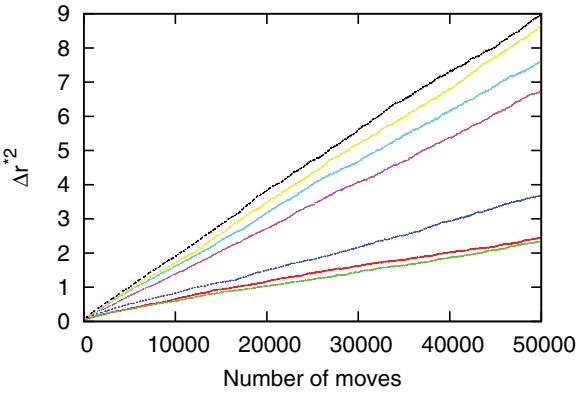

FIG. 7. (Color online) Average mean square particle displacement as a function of moves per particle for $T^* = 0.610$. Curves from the bottom up are for densities of 0.57, 0.58, 0.59, 0.60, 0.61, 0.62, and 0.63. In this system we have 300 particles.

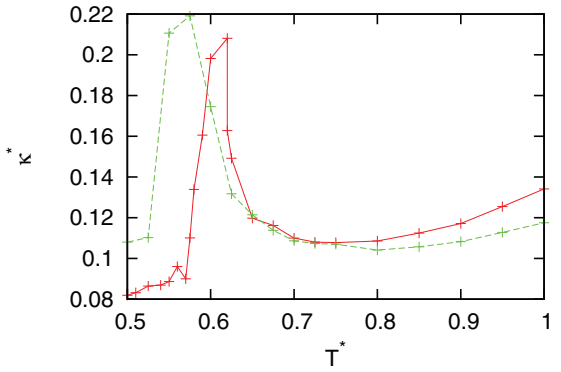

FIG. 10. (Color online) Temperature dependence of the thermal expansion coefficient at constant pressure for $p^* = 0.6$ (red) and $p^* = 0.75$ (green).

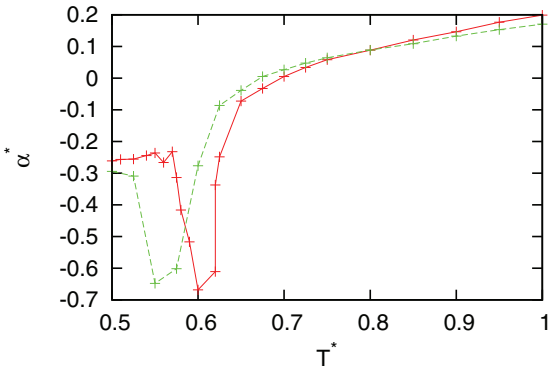

FIG. 11. (Color online) Temperature dependence of isothermal compressibility at constant pressure for $p^* = 0.6$ (red) and $p^* = 0.75$ (green).

Because of all this the critical point is shifted as compared to the infinite system.

Next we estimated the liquid-liquid critical point, which was a more difficult task because at these isotherms at lower densities the system splits into two phases (gas and liquid), while at higher densities it freezes. Figure 4 shows isotherms around the liquid-liquid critical point for 200 particles in the simulation box, and Fig. 5 shows a calculation of the thermodynamic limit. Note that the thermal expansion coefficient is negative in this region, which is the reason for the isotherms to move in the opposite direction than at the first critical point. Below critical temperature, the isotherms display a typical oscillating middle section where pressure decreases as density increases. This unstable portion of the phase diagram is compensated for using the Maxwell construction. The plotted coexistence curve connects the vertices of the Maxwell lines. The critical point, by definition, is the saddle on the critical isotherm, where $(\frac{\partial p}{\partial T})_V = (\frac{\partial^2 p}{\partial T^2})_V = 0$. On the interpolated polynomial curves fitted to the data we estimated a critical point for different sizes of the system and then calculated the thermodynamic limit. In this thermodynamic limit we ascertained that the liquid-liquid critical point (C2) is at $T^*_{C2} = 0.535 \pm 0.004$, $p^*_{C2} = 0.583 \pm 0.004$, and $\rho^*_{C2} = 0.591 \pm 0.005$. We have to mention that for smaller sizes ($N = 100$) the liquid-liquid phase transition is absent and it appears bigger only for systems of particles (in our case 200 particles or more). We checked accuracy of the liquid-liquid critical

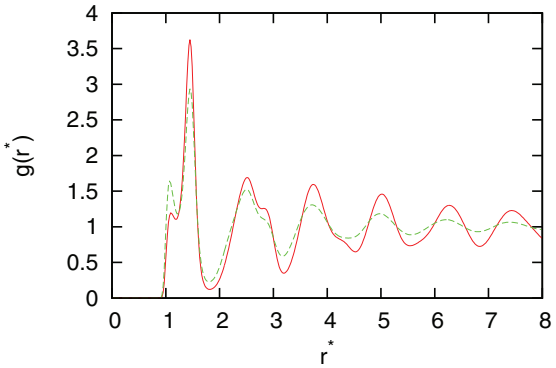

FIG. 12. (Color online) Pair distribution functions at $T^* = 0.65$ (green) and at $T^* = 0.6$ (red) at pressure $p^* = 0.6$.

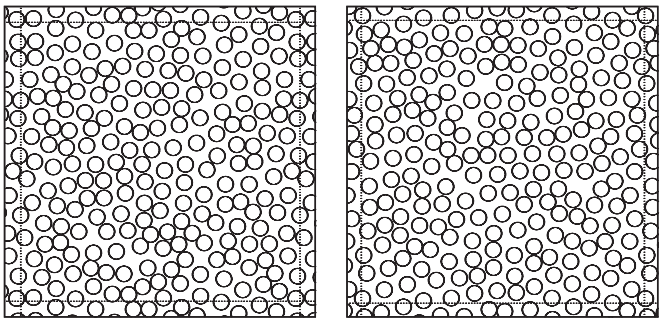

FIG. 13. Snapshots of the system for $p^* = 0.6$, $T^* = 0.6$ (left) and $p^* = 0.6$, $T^* = 0.65$ (right).

point by examining other properties. In the *NVT* ensemble we checked the heat capacity and mean square displacement of the particles. Figure 6 shows the heat capacity at constant volume for a system of 300 particles for temperatures below ($T^* = 0.610$) and above ($T^* = 0.611$) the critical point. There is a peak at the critical density for the liquid-liquid phase transition, but for temperatures lower than critical we observed different kinds of fluid for low densities. In Fig. 7 we plotted the average mean square displacement of particles as a function of moves per particle for simulation of a 300-particle system. Results are presented for different densities for temperatures below the critical point ($T^* = 0.610$). We can see that we have two different kinds of fluids, one at low densities and one at high.

In the *NpT* ensemble we checked the temperature dependence of density (Fig. 8), heat capacity at constant pressure (Fig. 9), the thermal expansion coefficient (Fig. 10), and isothermal compressibility (Fig. 11) as a function of temperature at constant pressure. Plotted are MC simulation data for a system of 200 particles. From these figures we can see that at higher temperatures we have a high-density fluid which changes to low-density fluid, and at very low temperatures the system starts to freeze. For the end we also plotted the radial distribution function (Fig. 12) and snapshots (Fig. 13) of low-density and high-density fluid. From the radial distribution function we can see that low-density fluid (red curve) has a longer range of correlations compared to a high-density fluid (green curve).

In our simulations we observed three different crystal phases. At low pressures ($p^* < 0.9$) molecules freeze in low-density hexagonal solid phase, at mid-range pressures we observed a cubic solid phase, and at very high pressures ($p^* > 10$) we also observed a high-density hexagonal solid phase. All this is in agreement with results by Almudallal *et al.* [14], where they observed all these phases for a similar square-shoulder square-well potential. They also observed two additional phases which we did not observe for the continuous version.

V. CONCLUSIONS

We have studied the phase diagram of two-dimensional particles interacting through a smooth version of the Stell-Hemmer interaction using Monte Carlo computer simulations. By analyzing the pressure-density isotherms and the temperature-density isobars we observed liquid-liquid, liquid-gas phase transitions and three stable crystal phases. We clearly observed the liquid-liquid phase transition in

the one-component system, and this was confirmed by all calculated properties. The state points inside the coexistence region separate into two phases characterized by different densities and structures. We also estimated liquid-gas and liquid-liquid critical points within the thermodynamic limit.

ACKNOWLEDGMENTS

We appreciate the support of the Slovenian Research Agency (P1 0103-0201 and J1 4148) and NIH Grant No. GM063592.

[1] P. C. Hemmer and G. Stell, Phys. Rev. Lett. **24**, 1284 (1970).
[2] A. B. de Oliveira, P. A. Netz, and M. C. Barbosa, Eur. Phys. J. B **64**, 481 (2008).
[3] R. Sharma, S. N. Chakraborty, and C. Chakravarty, J. Chem. Phys. **125**, 204501 (2006).
[4] Y. D. Fomin, V. N. Ryzhov, and E. E. Tareyeva, Phys. Rev. E **74**, 041201 (2006).
[5] S. Sastry and C. A. Angell, Nat. Mater. **2**, 739 (2003).
[6] C. A. Angell, R. D. Bressel, M. Hemmati, E. J. Sare, and J. C. Tucker, Phys. Chem. Chem. Phys. **2**, 1559 (2000).
[7] K. K. Mon, N. W. Ashcroft, and G. V. Chester, Phys. Rev. B **19**, 5103 (1979).
[8] D. Levesque and J. J. Weis, Phys. Lett. A **60**, 473 (1977).
[9] P. T. Cummings and G. Stell, Mol. Phys. **43**, 1267 (1981).
[10] A. Voronel, I. Paperno, S. Rabinovich, and E. Lapina, Phys. Rev. Lett. **50**, 247 (1983).
[11] E. Velasco, L. Mederos, G. Navascues, P. C. Hemmer, and G. Stell, Phys. Rev. Lett. **85**, 122 (2000).
[12] P. H. Poole, F. Sciortino, U. Essmann, and H. E. Stanley, Nature (London) **360**, 324 (1992).
[13] S. V. Buldyrev, G. Franzese, N. Giovambattista, G. Malescio, M. R. Sadr-Lahijany, A. Scala, A. Skibinsky, and H. E. Stanley, Physica A **304**, 23 (2002).
[14] A. M. Almudallal, S. V. Buldyrev, and I. Saika-Voivod, J. Chem. Phys. **137**, 034507 (2012).
[15] T. Urbic, J. Chem. Phys. **139**, 164515 (2013).
[16] P. Vilaseca and G. Franzese, J. Non-Cryst. Solids **357**, 419 (2011).
[17] A. B. de Oliveira, G. Franzese, P. A. Netz, and M. C. Barbosa, J. Chem. Phys. **128**, 064901 (2008).
[18] P. Vilaseca and G. Franzese, J. Chem. Phys. **133**, 084507 (2010).
[19] G. Franzese, J. Mol. Liq. **136**, 267 (2007).
[20] O. Pizio, H. Dominguez, Y. Duda, and S. Sokolowski, J. Chem. Phys. **130**, 174504 (2009).
[21] N. V. Gribova, Y. D. Fomin, D. Frenkel, and V. N. Ryzhov, Phys. Rev. E **79**, 051202 (2009).
[22] Z. Yan, S. V. Buldyrev, N. Giovambattista, P. G. Debenedetti, and H. E. Stanley, Phys. Rev. E **73**, 051204 (2006).
[23] P. Kumar, S. V. Buldyrev, F. Sciortino, E. Zaccarelli, and H. E. Stanley, Phys. Rev. E **72**, 021501 (2005).
[24] N. Choudhury and S. K. Ghosh, Phys. Rev. E **66**, 021206 (2002).
[25] G. Franzese, G. Malescio, A. Skibinsky, S. V. Buldyrev, and H. E. Stanley, Nature (London) **409**, 692 (2001).
[26] M. R. Sadr-Lahijany, A. Scala, S. V. Buldyrev, and H. E. Stanley, Phys. Rev. Lett. **81**, 4895 (1998).
[27] M. R. Sadr-Lahijany, A. Scala, S. V. Buldyrev, and H. E. Stanley, Phys. Rev. E **60**, 6714 (1999).
[28] A. Scala, M. R. Sadr-Lahijany, N. Giovambattista, S. V. Buldyrev, and H. E. Stanley, Phys. Rev. E **63**, 041202 (2001).
[29] D. Frenkel and B. Smit, *Molecular Simulation: From Algorithms to Applications* (Academic Press, New York, 2000).
[30] K. A. T. Silverstein, A. D. J. Haymet, and K. A. Dill, J. Am. Chem. Soc. **120**, 3166 (1998).